References

BASS, A. M. & BROIDA, H. P. (1956). *Phys. Rev.* **101**, 1740.

BOLZ, L. H., BOYD, M. E., MAUER, F. A. & PEISER, H. S. (1959). *Acta Cryst.* **12**, 247.

BROIDA, H. P. & PEYRON, M. (1957). *J. Phys. Radium*, **18**, 593.

BROIDA, H. P. & PEYRON, M. (1958). *J. Phys. Radium*, **19**, 480.

EDWARDS, O. S. & LIPSON, H. (1942). *Proc. Roy. Soc.* A, **180**, 268.

Encyclopedia of Physics (1957). XXXII, 451. Edited by S. FLÜGGE.

FIGGINS, B. F., JONES, G. O. & RILEY, D. P. (1956). *Phil. Mag.* 8/1, 747.

FONER, S. N., MAUER, F. A. & BOLZ, L. H. (1959). (The National Bureau of Standards, Washington, D.C.) Private communication.

HERZBERG, G. (1955). *Spectra of Diatomic Molecules*, London.

HERZFELD, C. M. & BROIDA, H. P. (1956). *Phys. Rev.* **101**, 606.

HERZFELD, C. M. (1957). *Phys. Rev.* **107**, 1239.

HOSEMANN, R. & BAGCHI, S. N. (1954). *Phys. Rev.* **94**, 71.

HÖRL, E. M. & MARTON, L. (1958). *Rev. Sci. Instrum.* **29**, 859.

HÖRL, E. M. (1959). *J. Mol. Spec.* **3**, 425.

KIMOTO, K. (1953). *J. Phys. Soc. Jap.* **8**, 762.

MAYER, H. (1929). *Z. Phys.* **58**, 373.

PATERSON, M. S. (1952). *J. Appl. Phys.* **23**, 805.

PEYRON, M. & BROIDA, H. P. (1959). *J. Chem. Phys.* **30**, 139.

PEYRON, M., HÖRL, E. M., BROWN, H. W. & BROIDA, H. P. (1959). *J. Chem. Phys.* **30**, 1304.

RUHEMANN, M. (1932). *Z. Phys.* **76**, 368.

SCHMID, E. & BOAS, W. (1935). *Kristallplastizität*, Berlin.

VEGARD, L. (1929). *Z. Phys.* **58**, 297.

WILSON, A. J. C. (1942). *Proc. Roy. Soc.* A, **180**, 277.

Acta Cryst. (1961). **14**, 19

Magnetic Structures of 3*d* Transition Metal Double Fluorides, K*Me*F$_3$*

BY VLADIMIRO SCATTURIN,† LESTER CORLISS, NORMAN ELLIOTT AND JULIUS HASTINGS

Department of Chemistry, Brookhaven National Laboratory, Upton, Long Island, New York, U.S.A.

(*Received* 23 *October* 1959 *and in revised form* 6 *February* 1960)

The antiferromagnetic structures of $KCrF_3$, $KMnF_3$, $KFeF_3$, $KCoF_3$, $KNiF_3$, and $KCuF_3$, have been obtained by neutron diffraction. The Mn, Fe, Co, and Ni double fluorides exhibit an ordering in which the divalent 3*d* ion is coupled antiferromagnetically to its six nearest neighbors. In the chromium double fluoride, the magnetic structure consists of ferromagnetic (001) sheets, coupled antiferromagnetically along the [001] direction. No magnetic scattering is observed in the neutron diffraction pattern of the copper double fluoride.

The magnetic structures and the observed crystallographic distortions are discussed in terms of an indirect exchange mechanism and in terms of the crystal field theory, respectively.

Introduction

Ionic compounds of formula ABX_3 often crystallize in the perovskite structure, provided the A and X ions form close-packed AX_3 layers and the B ion can be accommodated in the holes between these layers. When magnetically active B ions are introduced into this structure, there is a possibility of interaction leading to magnetic ordering. Antiferromagnetic structures have, indeed, been observed in perovskite-like double oxides of 3*d* trivalent ions: the so-called A-type configuration was observed for Mn^{+3} in $LaMnO_3$ (Wollan & Koehler, 1955) while the G-type was found for Mn^{+4} in $CaMnO_3$ (Wollan & Koehler, 1955), for Fe^{+3} and Cr^{+3} in $LaFeO_3$ and $LaCrO_3$ (Koehler & Wollan, 1957). Similar magnetic configurations were observed in the trifluorides of 3*d* transition metals (Wollan, Child, Koehler & Wilkinson, 1958), which have a crystal structure related to the perovskite structures. Indirect exchange interactions, depending on the electronic configuration of the ions and the crystal structure, presumably account for the magnetic ordering of these compounds. As in all indirect exchange couplings the anions play an important rôle in the exchange interaction.

A neutron diffraction study has been made of the magnetic structures of 3*d* metal double fluorides, K*Me*F$_3$, containing divalent magnetic ions and having a perovskite-like structure. The main purposes of this study were to find the magnetic ordering of the metal ions and to correlate the spin arrangement with the properties of the orbitals involved in the indirect exchange.

3*d* divalent ions and crystal field theory

It is convenient, for the subsequent discussion, to review at this point the properties of 3*d* divalent ions

* Research performed under the auspices of the U.S. Atomic Energy Commission.

† Present address: Istituto di Chimica Generale e Inorganica, Universita di Padova, Padova (Italy).

Table 1. *Electronic configurations and number of unpaired electrons in 3d divalent ions in octahedral coordination*

Ion	No. of 3*d* electrons	Configuration t_{2g}	Configuration e_g	No. of unpaired electrons t_{2g}	No. of unpaired electrons e_g	Total unpaired electrons
Cr^{+2}	4	3	1	3	1	4
Mn^{+2}	5	3	2	3	2	5
Fe^{+2}	6	4	2	2	2	4
Co^{+2}	7	5	2	1	2	3
Ni^{+2}	8	6	2	0	2	2
Cu^{+2}	9	6	3	0	1	1

and the crystal structures of perovskite-like compounds. The 3*d* level of a free transition divalent ion is split by the electric field due to negative charges or dipoles surrounding the cation in a crystal or complex. In a field of octahedral symmetry the splitting gives rise to two groups of levels: a lower triplet (t_{2g}) and an upper doublet (e_g). For tetrahedral symmetry these levels are inverted. The former case is realized for the *B* cations in a perovskite structure.

The orbitals associated with t_{2g} are directed toward the midpoints of the edges of a cube whose axes are the 4-fold symmetry axes of the surrounding octahedron or tetrahedron of anions; the e_g orbitals point along the axes, i.e. towards the face centers. The energy gap between the t_{2g} and e_g levels depends, among other things, upon the electronegativity of the anions, and the charge of the cation. For the oxides, for instance, it was found (Dunitz & Orgel, 1957*a*) that the separation for trivalent 3*d* ions is approximately twice the separation for the iso-electronic divalent 3*d* ions, despite a rather wide range of energy differences between levels (Dunitz & Orgel, 1957*b*). The fluoride ion is strongly electronegative and therefore the splitting produced by it will be rather small. In the corresponding weak field the distribution of electrons in the t_{2g} and e_g orbitals will, in general, be such as to give the maximum multiplicity. Table 1 lists the electron distribution for 3*d* divalent ions in octahedral coordination, based on these assumptions.

A regular octahedron of anions has cubic symmetry and requires that the non-bonding 3*d* electrons of the coordinated cation be symmetrically distributed among the *d* orbitals. Cubic symmetry can be achieved in the configurations

$$d^0,\ (t_{2g})^3,\ (t_{2g})^3(e_g)^2,\ (t_{2g})^6(e_g)^2,\ (t_{2g})^6(e_g)^4,$$

but in all other configurations the electrons are unevenly distributed among the 3*d* orbitals. In the latter case a Jahn–Teller effect will be operative (Dunitz & Orgel, 1957*a*). It is evident from Table 1 that d^4 and d^9 configurations will have large Jahn–Teller effects. Therefore, hexa-coordinated Cr^{+2} and Cu^{+2} compounds would be expected to have rather large anion distortions, whereas no Jahn–Teller distortion will be present in Mn^{+2}, Fe^{+2}, Co^{+2} and Ni^{+2} compounds with half filled e_g orbitals.

Crystal structure of perovskite-like compounds

Ionic ABX_3 compounds with the ideal perovskite structure, have cubic stacking of close-packed AX_3 layers, with octahedral anion holes occupied by the *B* ion. This structure is often found to be distorted, especially when the *A* and *B* cations do not satisfy the tolerance conditions for being in dodecahedral and octahedral coordination, respectively.

In transition metal perovskites two kinds of distortions were discovered recently; one in double oxides of rare earths and trivalent 3*d* ions (Geller, 1956; Geller & Wood, 1956; Geller & Bala, 1956; Gilleo, 1957; Geller, 1957), the other in $KCuF_3$ by Knox (1959). Both modifications are subgroups of *m*3*m*, the point group of the ideal perovskite.

A perovskite-like structure has also been observed for the 3*d* transition metal double fluorides, K*Me*F$_3$ (Martin, Nyholm & Stephenson, 1956). In this case the potassium and fluorine ions form close-packed layers and the octahedral holes can accommodate cations of radii between 0·543 and 1·02 Å. Divalent transition ions, with $3d^4$ through $3d^9$ configurations, lie within this range. It has to be recalled, however, that the electronic configuration of $Cr^{+2}(d^4)$ and $Cu^{+2}(d^9)$ is stabilized by a non-cubic crystal field so that the fluorine octahedron surrounding these ions will tend, generally, to be tetragonally distorted.

Experimental

Sample preparations and magnetic properties

Double fluorides of K and Cr^{+2}, Mn^{+2}, Fe^{+2}, Co^{+2}, Ni^{+2}, and Cu^{+2} were prepared by precipitation, adding an aqueous solution of the divalent 3*d* ions to an acidified solution of potassium fluoride (Palmer, 1954). Particular care was taken to avoid oxidation in precipitating the Cr and Fe compounds. The analysis of the constituents of the dried powders showed that Fe and Ni double fluorides were non-stoichiometric, with an excess of potassium and a deficiency of transition metal and fluorine, with the latter pair, however, in the ratio 1:3. A small amount of H_2O was inferred, from the analytical data, in the Ni salt. X-ray powder diagrams of the non-stoichiometric compounds showed only the lines of the perovskite structure and therefore the crystal was considered disordered, with some H_2O statistically distributed in the KF_3 layers and random vacancies in the transition metal sites.

The magnetic susceptibility measurements of Martin, Nyholm & Stephenson (1956) and Ogawa (1959) show that $KMnF_3$, $KFeF_3$, $KCoF_3$, $KNiF_3$, and $KCuF_3$

Table 2. *Néel temperatures of transition metal double fluorides,* $KMeF_3$

Compound	$KMnF_3$	$KFeF_3$[b]	$KCoF_3$[b]	$KNiF_3$[b]	$KCuF_3$[b]
T_N in °K.	95; 89[a] 88·3[c]	115	135	275	< 100

(*a*) Ogawa (1959). (*b*) Martin, Nyholm & Stephenson (1956). (*c*) Shulman, Knox & Wyluda (1959).

are antiferromagnetic with Néel temperatures given in Table 2. Nuclear magnetic resonance measurements by Shulman *et al.* (1959) also show that $KMnF_3$ is antiferromagnetic.

Neutron diffraction powder patterns

Neutron diffraction patterns at 1·064 Å were obtained for powder samples of $KCrF_3$, $KMnF_3$, $KFeF_3$, $KCoF_3$, $KNiF_3$, and $KCuF_3$ at room, liquid nitrogen and liquid helium temperatures using an aluminum cell. In addition, patterns were obtained in a quartz cell at room temperature in order to eliminate the aluminum interferences.

The observed integrated intensities were compared with $jF^2_{calc.}$ after correction for scale, Lorentz, and temperature factors. In the case of the Fe and Ni salts, the result of the chemical analysis was taken into account in the computation of $F^2_{calc.}$. The scattering amplitudes were obtained from a recent compilation of scattering cross sections (Hughes & Schwartz, 1958) with the exception of Co, for which an amplitude of $0{\cdot}25 \times 10^{-12}$ cm. was adopted (Roth, 1958). The magnetic peak intensities were normalized internally by comparison with the strongest nuclear reflection in order to fix the magnetic moments and 3*d* electron form factors.

Neutron diffraction data and antiferromagnetic structure

$KFeF_3$, $KCoF_3$, and $KNiF_3$.—Neutron diffraction patterns for these three compounds at 4·2 °K. are shown in Fig. 1. In comparison with the room temperature patterns, they show magnetic superlattice lines, which can be indexed on a cubic unit cell with twice the edge of the corresponding perovskite unit cell. The parameters obtained from the high angle lines of the liquid helium neutron patterns are as follows:

	$KNiF_3$	$KCoF_3$	$KFeF_3$
a_0 (Å)	$7{\cdot}98_6$	$8{\cdot}08_4$	$8{\cdot}17_6$

The ratio of the nuclear intensities at 4·2 °K. and room temperature varies with $\sin^2\theta$ according to the usual exponential law, which shows that no phase change has occurred at low temperature and that there is no magnetic scattering superimposed on the nuclear reflections with all even (*hkl*) indices. This absence of magnetic scattering at the nuclear positions can be interpreted as an extinction rule of the magnetic lattice. Since the magnetic ions alone contribute to the pattern, they must be arranged in a face centered NaCl-type lattice, with the alkali and halogen ions corresponding to oppositely directed moments. The

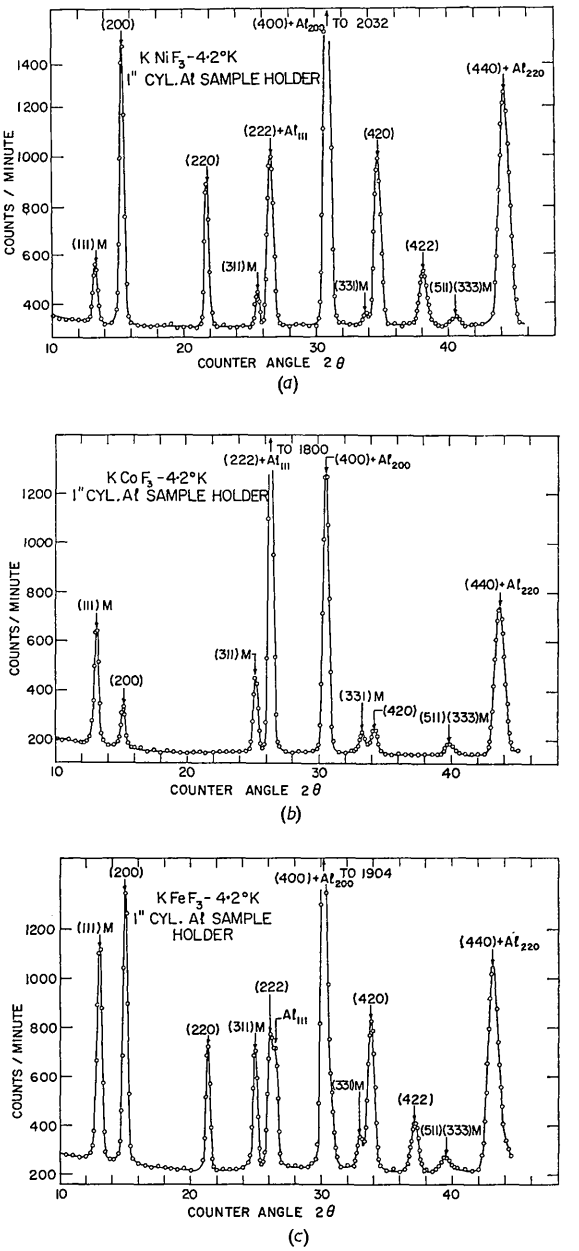

Fig. 1. Neutron diffraction patterns of $KNiF_3$, $KCoF_3$ and $KFeF_3$.

antiferromagnetic arrangement consists of spins alternating along the three directions of a cube, twice the edge of the perovskite unit cell.

The configurational symmetry (Shirane, 1959) of the magnetic structure is cubic and therefore it is im-

possible, from powder data, to find the spin directions relative to the crystallographic directions. The calculated magnetic intensities, using the Mn^{+2} form factor (Hastings, Elliott & Corliss, 1959), are systematically smaller than the observed values. Normalization to the nuclear peaks shows that the magnetic form factors of Fe^{2+}, Co^{2+} and Ni^{2+} fall off less rapidly with angle, and in the order Mn^{+2}, Fe^{+2}, Co^{+2}, Ni^{+2}, which is also the order of the effective atomic number.

The experimental magnetic form factors are plotted in Fig. 2 as a function of $4\pi\ (\sin\theta/\lambda)$. Table 3 lists the observed magnetic scattering amplitudes and corresponding magnetic moments.

Table 3. *Observed magnetic scattering amplitudes and corresponding magnetic moments for* $KFeF_3$, $KCoF_3$, *and* $KNiF_3$

Compound	Ion	$p \times 10^{12}$ cm.	Moment in μ_β
$KFeF_3$	Fe^{+3}	0·974	4·42
$KCoF_3$	Co^{+2}	0·735	3·33
$KNiF_3$	Ni^{+2}	0·490	2·22

$p = (e^2\gamma/2mc^2)gS = 0{\cdot}2695gS \times 10^{-12}$ cm.

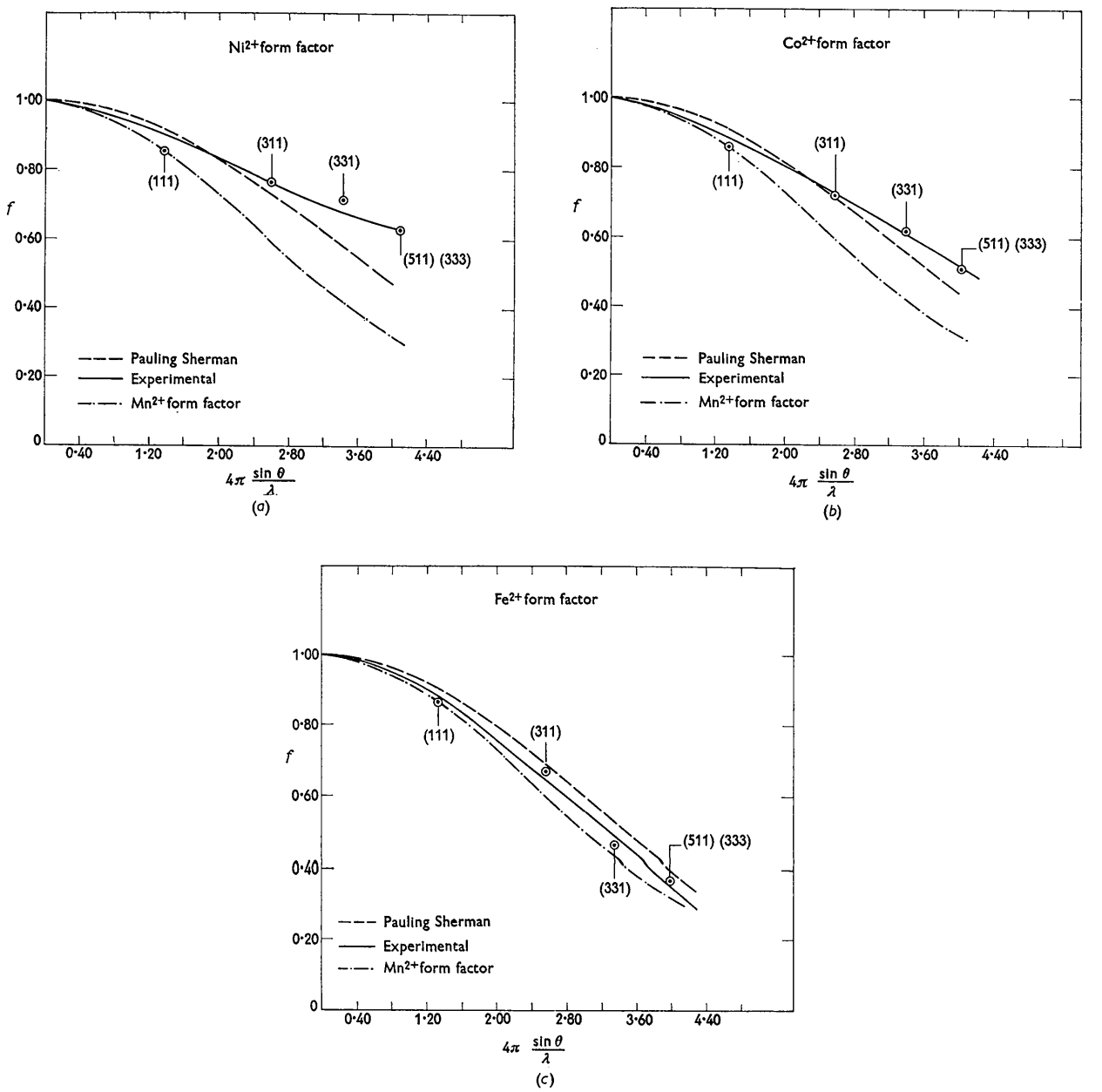

Fig. 2. Composite magnetic form factors for Ni^{+2}, Co^{+2}, and Fe^{+2}. The Pauling–Sherman form factors are computed as explained in the text. The Mn^{+2} form factor is taken from Hastings, Elliott & Corliss (1959).

Table 4. *Calculated and observed intensities for* $KNiF_3$, $KCoF_3$, *and* $KFeF_3$

Nuclear peaks

Magnetic cell cubic indices	$KNiF_3$			$KCoF_3$		$KFeF_3$		
	$I_c^{(a)}$	$I_c'^{(b)}$	I_o	I_c	I_o	$I_c^{(a)}$	$I_c'^{(b)}$	I_o
200	2199	2065	1866	254	254	1946	1724	1752
220	982	875	923	~0	0	835	793	762
222	594	761	742	1788	1725	694	854	875
400	3356	3319	3468	1644	1580	3160	3233	3272
420	1658	1599	1599	210	221	1548	1391	1392
422	622	559	663	~0	0	550	529	507
440	3045	3184	3200	1632	1607	3097	3244	3379

Magnetic peaks

Magnetic cell cubic indices	$KNiF_3$		$KCoF_3$		$KFeF_3$	
	I_c'	I_o	I_c	I_o	I_c'	I_o
111	450	403	857	843	1665	1600
311	270	275	502	497	791	821
331	130	143	214	221	257	228
511, 333	107	105	145	144	125	143

(*a*) I_c was computed on the basis of the stoichiometric $KMeF_3$ formula.
(*b*) I_c' was computed on the basis of the analytical formulas, $KNi_{0.922}F_{2.91}(H_2O)_{0.10}$ and $KFe_{0.872}F_{2.79}$.

The experimental form factors in Fig. 2 are compared with computed Pauling & Sherman (1932) form factors, obtained from 3*d* hydrogen-like functions and Hartree (1957) screening constants for Fe^{+2}, Co^{+2} and Ni^{+2} ions. The magnetic moments show orbital contributions and they are in agreement with previous neutron diffraction data of Erikson (1952) on the corresponding difluorides and of Roth (1958) for Ni^{+2} in the oxide.

The observed and calculated intensities are compared in Table 4. The nuclear components were calculated on the basis of the perovskite structure. Calculated intensities are listed for both a stoichiometric formula and for a composition corresponding to the chemical analysis.

The magnetic components were calculated using the experimental magnetic amplitude and assuming, for the $KNiF_3$ and $KFeF_3$ salts, vacancies randomly distributed among the metal sites.

$KMnF_3$.—The neutron diffraction pattern of $KMnF_3$ at 4·2 °K. is shown in Fig. 3. In comparison with the room temperature data, this pattern shows the same superlattice magnetic reflections as the previous double fluorides, but, in addition, two small peaks around the (222) nuclear reflection. All the lines can be indexed on a cubic unit cell of $8{\cdot}31_8$ Å, twice the edge of the corresponding perovskite unit cell.

Comparison of liquid He and room temperature nuclear intensities shows that the structure is modified at 4·2 °K. and the change in intensities can be accounted for on the basis of small movements of the atoms from the ideal perovskite positions. The magnetic peak positions and intensities indicate, however, no departure of the Mn^{+2} ions from the ideal parameters. The appearance of the small (310) and (321) lines mentioned above and the general lack of agreement between observed and calculated nuclear intensities show that the potassium and fluorine ions are involved in the distortion. The limited number of lines of the neutron diffraction pattern and the severe overlap of different reflections, due to the cubic relationship of the lattice parameters, preclude a precise atomic parameter determination. In any event fairly good agreement between observed and calculated intensities was obtained on the basis of Geller's (1956) model of the distortion of the perovskite structure. The fluorine octahedra alone were tilted, maintaining, for one set of fluorine parameters, the values obtained by Gilleo (1957) for O_I^{-2} in $La(Co_{0.2}Mn_{0.8})O_3$ and assuming, for the other F^- set, values smaller than the O_{II}^{-2} parameters. The observed and calculated intensities for $KMnF_3$ nuclear peaks are reported in Table 5.

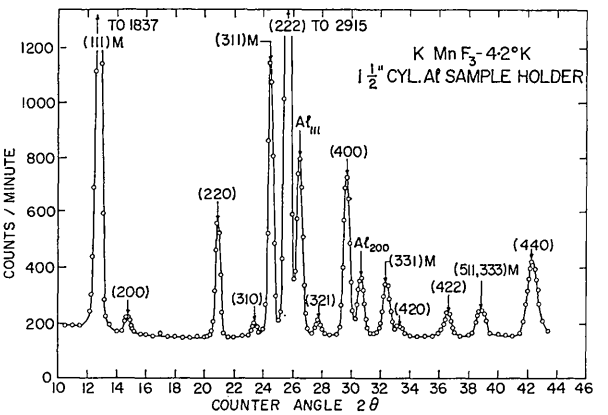

Fig. 3. Neutron diffraction pattern of $KMnF_3$.

The previously discussed distortion does not affect the magnetic structure because the Mn^{+2} ions are still in a cubic arrangement and the superlattice lines can be accounted for in the same way as in $KFeF_3$, $KCoF_3$ and $KNiF_3$, with an identical spin configuration. The

Table 5. *Calculated and observed nuclear intensities for* KMnF$_3$*

Magnetic cell cubic indices	Orthorhombic *Pnma* indices	I_c	I_o
200	101, 020	104	93
220	002, 200, 121	658	641
310	102, 201	50	69
311	130, 031, 112, 211	15	obscured
222	022, 220	4387	4655
321	122, 221	55	97
400	040, 202	1059	1151
420	103, 301, 222, 141	91	112
422	321, 123, 240, 042	293	246
440	400, 004, 242	783	840

* The nuclear intensities of KMnF$_3$ were calculated with the following parameters of the *Pnma* space group:

4 K$^+$ in 4(*c*) $\pm(x, \frac{1}{4}, z;\ \frac{1}{2}+x, \frac{1}{4}, \frac{1}{2}-z)$ $x=0$; $z=0$.

4 Mn^{2+} in 4(*b*) 0, 0, $\frac{1}{2}$; 0, $\frac{1}{2}$, $\frac{1}{2}$; $\frac{1}{2}$, 0, 0; $\frac{1}{2}$, $\frac{1}{2}$, 0.

4 F_I^- in 4(*c*) $\pm(x, \frac{1}{4}, z;\ \frac{1}{2}+x, \frac{1}{4}, \frac{1}{2}-z)$ $x=0{\cdot}500$; $z=0{\cdot}010$.

8 F_{II}^- in 8(*d*) $\pm(x, y, z;\ \frac{1}{2}+x, \frac{1}{2}-y, \frac{1}{2}-z;\ x, \frac{1}{2}+y, z;\ \frac{1}{2}-x, y, \frac{1}{2}+z)$ $x=0{\cdot}260$; $y=0{\cdot}040$; $z=-0{\cdot}270$.

The transformation matrices *Pbnm* → *Pnma* are as follows:

(*a*) *Indices* 001/100/010; (*b*) *Coordinates* 010/001/100.

Table 6. *Calculated and observed magnetic intensities for* KMnF$_3$

Indices mag. cubic cell	I_c	I_o
111	3259	3108
311	1381	1476
331	429	419
511, 333	223	280*

* The (511, 333) magnetic peak has superimposed an orthorombic nuclear component.

observed form factor is in agreement with the Mn^{+2} form factor and a magnetic moment of 5·06 μ_β was found. The observed and calculated magnetic intensities are compared in Table 6.

KCuF$_3$.—The neutron diffraction pattern of KCuF$_3$ at 4·2 °K. is presented in Fig. 4. No superstructure

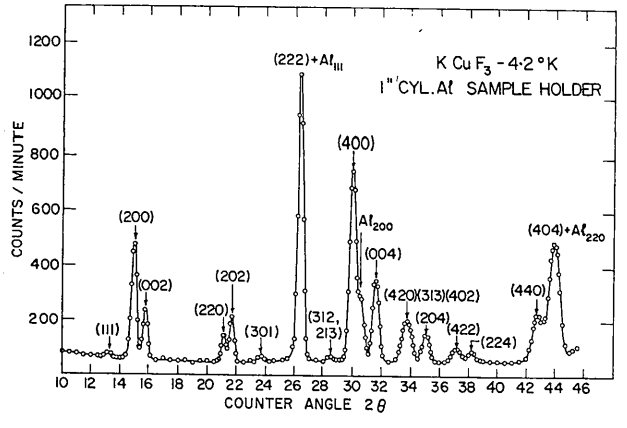

Fig. 4. Neutron diffraction pattern of KCuF$_3$.

lines were observed. The pattern can be indexed on the basis of a tetragonal unit cell having

$$a=8{\cdot}20_2,\ c=7{\cdot}81_8\ \text{Å}.$$

If the small peaks at 23·7° and 28·5° in 2θ are not considered, the (*hkl*) indices of the pattern are all even or all odd, indicating a face centered tetragonal unit cell with lattice constants twice that of a distorted perovskite cell. The distortion in this case is more pronounced than in KMnF$_3$ and involves lattice dimensions as well as atomic positions.

Table 7. *Calculated and observed nuclear intensities for* KCuF$_3$

Indices F_{cell}	I_{cell}	$I_{calc.}$	$I_{obs.}$
200	110	788	996
002	002	307	
220	020	119	385
202	112	229	
222	022	651	686
400	220	1302	1389
004	004	567	636
420	130	8	461
313	123	24	
402	222	244	
204	114	240	229
422	132	136	220
224	024	128	
440	040	614	2156*
404	224	1174	

* The (404) observed intensity includes the Al_{220} peak.

In a very recent communication Knox (1959) reported some X-ray studies, at room temperature, of KCuF$_3$ as well as of the other double fluorides. The copper compound was found to belong to the *F*4*mc* space group with Cu^{+2}, K^{+1} and two sets of F^- in the special positions 8(*b*), 8(*a*), 8(*b*) and 16(*c*). A convenient cell transformation changes the *F*4*mc* space group into the standard *I*4*cm* space group, which is related to the orthorhombic modification observed by Geller (1956). The intensities of the neutron diffraction pattern of KCuF$_3$ at 4·2 °K. indicate that Knox's parameters are essentially correct. The presence of the small (301) and (312) peaks shows, however, that the cell is no longer body centered at liquid He temperature. Very small movements of the K and F atoms can destroy the $\frac{1}{2}$, $\frac{1}{2}$, $\frac{1}{2}$ superposition and lead to a primitive tetragonal or orthorhombic space group. The powder data are not capable of a definitive confirmation of the structure. In Table 7 observed intensities are compared with calculated ones, using the atomic parameters of Knox (1959).

KCrF$_3$.—The neutron diffraction pattern of KCrF$_3$ at 4·2 °K. is shown in Fig. 5. The pattern shows well defined magnetic superlattice lines which are not

present in the liquid N_2 data and all reflections can be indexed on the basis of a tetragonal unit cell of parameters $a=8{\cdot}54_4$, $c=7{\cdot}96_6$ Å. The indexing of the nuclear reflections is based on a primitive unit cell with twice the edges of a tetragonal perovskite unit cell. The nuclear intensities indicate that the movements of the atoms from the ideal perovskite positions are larger than in $KCuF_3$. Unfortunately, as was the case for the copper salt, the powder data alone are not capable of determining the parameters.

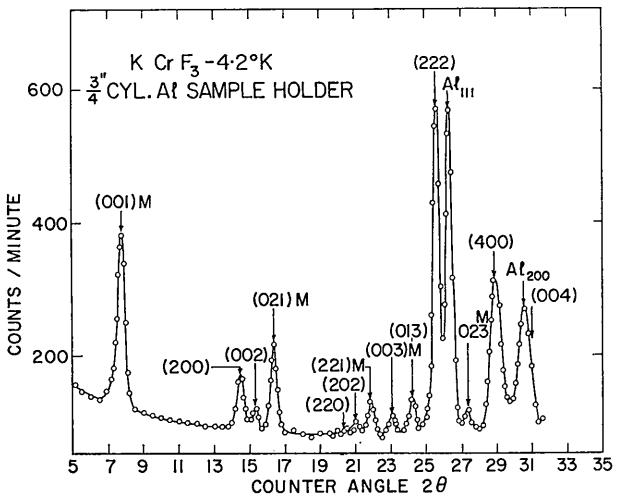

Fig. 5. Neutron diffraction pattern of $KCrF_3$.

The spin arrangement, however, can be deduced from the magnetic superlattice pattern, which shows only lines with h, k, even and $l=2n+1$. Therefore the Cr^{+2} ions form a tetragonal lattice with their spins parallel in the (001) plane, but alternating along the [001] direction. The magnetic structure is thus characterized by ferromagnetic Cr^{+2} sheets coupled antiferromagnetically. The configurational symmetry is such that only the angle between the moment direction and the c axis can be determined. The strong (001) line that is observed shows that the spins must lie close to the (001) plane. The magnetic peak intensities, calculated for a model with the spins placed in the (001) plane, are in good agreement with the observed intensities. The Mn^{+2} form factor was used in these calculations and the comparison is shown in Table 8. The normalization of the (001) magnetic peak with the (200)(002) nuclear peaks, assuming for $KCrF_3$ the same parameters as for $KCuF_3$, gives a Cr^{+2} magnetic moment of $4{\cdot}27\ \mu_\beta$.

Table 8. *Calculated and observed magnetic intensities for* $KCrF_3$

Indices magnetic tetr. unit cell	I_c	I_o
001	600	605
021	236	230
221	87	86
003	32	35
023	59	56

Discussion

The magnetic structures of 3*d* transition metal double fluorides are characterized by the so-called *A* and *G* arrangements (Fig. 6) discovered in the double oxides of trivalent 3*d* ions (Wollan & Koehler, 1955; Koehler & Wollan, 1957) and in the trifluorides of 3*d* ions (Wollan, Child, Koehler & Wilkinson, 1958). The *A*-type structure, which consists of ferromagnetic (001) sheets coupled antiferromagnetically along the [001] direction, is found in $KCrF_3$. In the *G*-type structure, the magnetic ion is coupled antiferromagnetically to its six nearest neighbors. This structure is found in $KMnF_3$, $KFeF_3$, $KCoF_3$, and $KNiF_3$.

The arrangement of the moments in the double fluorides is the expected one on the basis of an indirect exchange mechanism. The interactions are supposed to take place via the non-magnetic F^- anions, and the electronic configuration of the cations as well as the crystal structure determine the particular type of magnetic ordering. Hence the same interaction mechanism, which accounted for the magnetic structure of trivalent transition metal perovskites and the related trifluorides, is seen to explain the divalent transition metal double fluorides, provided one takes into consideration the change in the electronic structure.

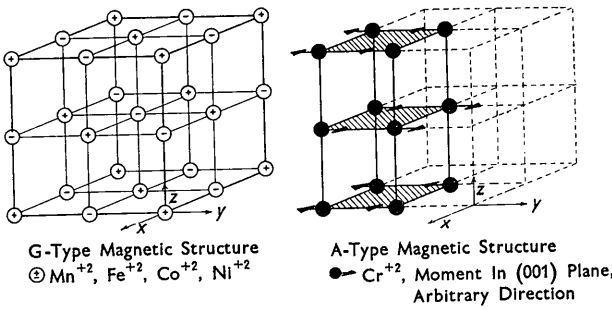

Fig. 6. *A* and *G* type magnetic structures in 3*d* transition metal double fluorides. In the *G* structure the parallel and antiparallel orientation of the moments are shown by positive and negative spheres. In the *A* structure, the direction of the magnetic axis relative to the crystallographic *c* axis is shown by an arrow.

In perovskite-like structures, where lines of anion octahedra run along the crystallographic directions, the indirect interactions will produce lines of alternating spins, along the same directions, with transition ions of d^3, and d^5 through d^8 configurations. This magnetic structure was found in $CaMnO_3$ (Wollan & Koehler, 1955), $LaFeO_3$, $LaCrO_3$ (Koehler & Wollan, 1957), CrF_3, FeF_3, CoF_3 (Wollan, Child, Koehler & Wilkinson, 1958), and now in $KMnF_3$, $KFeF_3$, $KCoF_3$, and $KNiF_3$.

In the d^4 configuration, the *p* orbitals of the anion

may overlap both half-filled and empty e_g orbitals of the cation. The overlap of the anion orbitals with a pair of half-filled or a pair of empty e_g cation orbitals, will lead to antiferromagnetic coupling, whereas an overlap of a mixed pair will lead to a ferromagnetic coupling. Therefore both *A* and *G*-type coupling schemes are possible for the d^4 configuration. Up to the present, the *A*-type structure accounts for all the experimental observations, namely $LaMnO_3$ (Wollan & Koehler, 1955), MnF_3 (Wollan, Child, Koehler & Wilkinson, 1958) and $KCrF_3$.

The crystallographic distortions found in $KCrF_3$ and $KCuF_3$, which contain ions with d^4 and d^9 configurations, are the expected ones on the basis of the Jahn–Teller effect. The magnetic structure of the chromium salt shows that the e_g orbitals must have the same orientation, with respect to the crystal axes, as was inferred in MnF_3 (Wollan, Child, Koehler & Wilkinson, 1958). The ratio $c/a < 1$ indicates that four anions are closer to the chromium ion than the other two.

In $KCuF_3$ there is no way of deducing the orientation of the 3*d* orbitals from the magnetic structure. The c/a ratio is, again, less than 1 and a Jahn–Teller distortion with d_{Z^2} orbitals singly occupied is rather improbable (Orgel & Dunitz, 1957). Therefore an orbital arrangement similar to $KCrF_3$ and MnF_3 is rather likely. If this is the case, and also if in the copper salt the superexchange mechanism is operative, one would expect lines of alternating spins along [001]. There does not seem to be any indirect exchange mechanism, however, which can provide coupling between these lines. This may be the reason for the absence of a magnetic structure in the neutron diffraction pattern of the copper double fluoride.

We wish to thank Dr R. W. Stoenner for the analysis of the samples and Mr David Langdon for running the neutron patterns. One of us (V. S.) was supported by an award from the National Academy of Sciences and the International Cooperation Administration, as a participant in the Scientist Research Project. The grant is gratefully acknowledged.

References

Dunitz, J. D. & Orgel, L. E. (1957*a*). *J. Phys. Chem. Solids*, **3**, 20.
Dunitz, J. D. & Orgel, L. E. (1957*b*). *J. Phys. Chem. Solids*, **3**, 318.
Erikson, R. A. (1952). Ph.D. Thesis.
Geller, S. (1956). *J. Chem. Phys.* **24**, 1236.
Geller, S. & Wood, E. A. (1956). *Acta Cryst.* **9**, 563.
Geller, S. & Bala, W. B. (1956). *Acta Cryst.* **9**, 1019.
Geller, S. (1957). *Acta Cryst.* **10**, 243.
Gilleo, M. A. (1957). *Acta Cryst.* **10**, 161.
Hartree, D. (1957). *The Calculations of Atomic Structures*. New York: Wiley.
Hastings, J. M., Elliott, N. & Corliss, L. M. (1959). *Phys. Rev.* **115**, 13.
Hughes, D. J. & Schwartz, R. B. (1958). *Neutron Cross Sections*, 2nd Ed. Upton, New York: Brookhaven National Laboratory.
Knox, K. (1959). Annual Meeting A.C.A., Ithaca, July 1959.
Knox, K. (1959). Private communication.
Koehler, W. C. & Wollan, E. O. (1957). *J. Phys. Chem. Solids*, **2**, 100.
Martin, R. L., Nyholm, R. S. & Stephenson, N. C. (1956). *Chem. Ind.* **3**, 38.
Ogawa, S. (1959). *J. Phys. Soc. Japan*, **14**, 1115.
Orgel, L. E. & Dunitz, J. D. (1957). *Nature, Lond.* **179**, 462.
Palmer (1954). *Experimental Inorganic Chemistry*. London: Cambridge University Press.
Pauling, L. & Sherman, J. (1932). *Z. Kristallogr.* **81**, 1.
Roth, W. L. (1958). *Phys. Rev.* **110**, 1333.
Shirane, G. (1959). *Acta Cryst.* **12**, 282.
Shulman, R. G., Knox, K. & Wyluda, B. J. (1959). *Bull. Amer. Phys. Soc.* **4**, 166.
Wollan, E. D. & Koehler, W. C. (1955). *Phys. Rev.* **100**, 345.
Wollan, E. D., Child, H. R., Koehler, W. C. & Wilkinson, H. K. (1958). *Phys. Rev.* **112**, 1132.